

# Photoluminescence enhancement and quenching of single CdSe/ZnS nanocrystals on metal surfaces dominated by plasmon resonant energy transfer

Kazunari Matsuda,<sup>a)</sup> Yuichi Ito, and Yoshihiko Kanemitsu<sup>b)</sup>

*Institute for Chemical Research, Kyoto University, Uji, Kyoto 611-0011, Japan*

(Received 6 March 2008; accepted 5 May 2008; published online 30 May 2008)

We studied the mechanism of the photoluminescence (PL) enhancement and quenching of single CdSe/ZnS nanocrystals on rough Au surfaces. Single nanocrystal spectroscopy revealed that the PL enhancement depends strongly on the excitation wavelength and liner-polarization angle due to the localized plasmon excitation and is also sensitive to the nanocrystal size. The polarization- and size-dependent PL enhancement and quenching are determined by the balance between the resonant energy transfer from the nanocrystal to the Au surface and the electric field enhancement. © 2008 American Institute of Physics. [DOI: 10.1063/1.2937142]

Chemically synthesized semiconductor nanocrystals have unique optical properties, such as high photoluminescence (PL) efficiencies and size-dependent PL wavelengths, and are among the most promising building blocks for nanoscale optoelectronic devices. The control of exciton states in nanocrystals is essential for the fabrication of devices, such as light-emitting diodes,<sup>1</sup> lasers,<sup>2</sup> and solar cells.<sup>3</sup> The excitonic responses of nanocrystals can be controlled via the charge and energy transfer at the interface between nanocrystals and the surrounding environment due to the large surface-to-volume ratios of nanocrystals. Drastic changes in the optical responses of nanocrystals are anticipated by controlling the nanoscale-localized energy transfer at the interface.

Very recently, interest from the fundamental physics viewpoints has grown in semiconductor/metal heterostructures including semiconductor nanocrystal/metal systems.<sup>4–12</sup> As the energy transfer between the excitons in the nanocrystal and plasmons in the metal surface occurs, the optical properties of nanocrystals near the metal surface are modified markedly. In fact, it has been shown that the PL enhancement and quenching of nanocrystals occur on metal substrates and near metal particles.<sup>8–12</sup> However, the PL enhancement or quenching changes sensitively depending on the conditions and its mechanism are not fully understood due to characteristics of the PL process. This involves the contributions of two complicated processes:<sup>13</sup> the modulated excitation process of the plasmon and the emission process influenced by the exciton energy transfer. The control of the energy transfer will provide us new physical aspects in semiconductor nanocrystal/metal heterostructures.

In this letter, we study mechanism of the PL enhancement and quenching of a single semiconductor nanocrystal on the rough metal surface by changing incident light polarization and nanocrystal size. A single nanocrystal spectroscopy and time-resolved spectroscopy reveal the contribution of excitation process and energy transfer process in the PL enhancement and quenching.

The average core sizes (diameter  $D$ ) of the CdSe/ZnS core/shell nanocrystals (Evident Technologies) used in this work were 5.2, 4.0, and 2.4 nm, and their respective PL wavelengths at room temperature were 620, 600, and 540 nm. The CdSe/ZnS nanocrystal solutions were dispersed directly on cover glasses or Au films with rough surfaces<sup>12</sup> using a spin-coating technique. Single nanocrystal PL measurements at room temperature were taken under a wide-field luminescence microscope with a objective (numerical aperture of 0.8). The nanocrystals were excited with a continuous-wave linear-polarized Ar<sup>+</sup> laser (457.9, 488, and 514.5 nm), a Nd<sup>3+</sup>:YVO<sub>4</sub> laser (532 nm), or a He–Ne laser (594 nm). The PL images were recorded using an electron-multiple charge-coupled device camera with a 50 ms exposure time. PL decay dynamics was studied under 150 fs, 490 nm laser excitation using a streak camera with the instrument response of about 70 ps.

Figures 1(a) and 1(b) show PL images of single CdSe/ZnS nanocrystals ( $D=5.2$  nm) on the glass and rough Au surfaces, respectively. These images with same vertical scales were obtained under liner-polarized 514.5 nm excitation. The PL intensities of single nanocrystals on the glass are roughly constant, while there is a significant intensity variation of each nanocrystal on the rough Au surface. About sixfold PL intensity enhancement is maximally observed on the rough Au surface and almost completely quenching is also observed in the same image. Figure 1(c) shows the typical PL intensities of a single nanocrystal on the Au and glass surface as a function of the excitation polarization angle. The PL intensity of a single nanocrystal on glass does not change with the polarization angle. Conversely, PL intensity on a rough Au surface oscillates with a period of 180° on the polarization angle and the PL intensity can be controlled by the polarization. The difference in the maximum and minimum values of the PL intensity are almost constant values of  $20 \pm 5$  times. It is found that the intensity variation on rough Au surface arises from strong polarization sensitivities of the PL intensities.

We measured the maximum PL intensity of a single nanocrystal with varying the polarization angle. The polarization dependence of PL intensity of a single nanocrystal with different size ( $D=4.0$  and 2.4 nm) on the rough Au surface also shows oscillation behavior (not shown here).

<sup>a)</sup>Electronic mail: matsuda@sci.kyoto-u.ac.jp.

<sup>b)</sup>Electronic mail: kanemitsu@sci.kyoto-u.ac.jp. Also at Photonics and Electronics Science and Engineering Center, Kyoto University, Kyoto 615-8510, Japan.

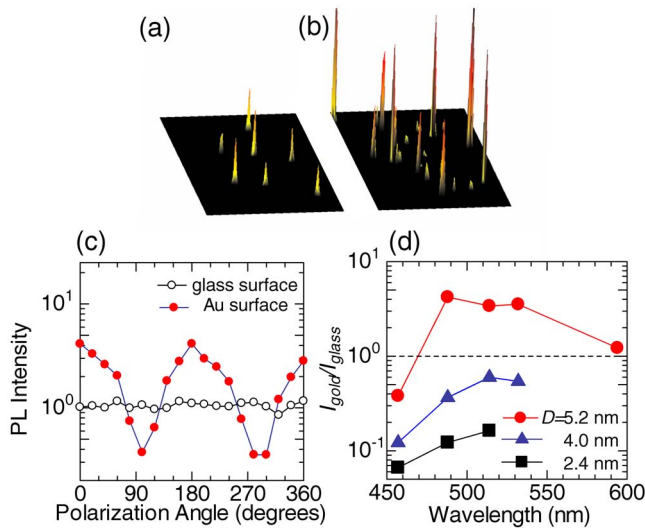


FIG. 1. (Color online) [(a) and (b)] PL images of single CdSe/ZnS nanocrystals ( $D=5.2$  nm) on glass and Au surfaces in a  $24 \times 27 \mu\text{m}^2$  area, respectively. The excitation power density was kept below  $300 \text{ W/cm}^2$ . (c) PL intensities of single nanocrystals ( $D=5.2$  nm) on rough Au and glass surfaces as a function of the linear-polarization angle. The vertical axis is shifted to show the PL intensity maximum at the origin in this single nanocrystal. (d) Nanocrystal size dependence of the PL intensity ratio ( $I_{\text{gold}}/I_{\text{glass}}$ ) as a function of the excitation wavelength.

Figure 1(d) shows the excitation wavelength dependence of the PL enhancement and quenching factor as  $I_{\text{gold}}/I_{\text{glass}}$ , where  $I_{\text{gold}}$  ( $I_{\text{glass}}$ ) is the maximum PL intensity on the Au surface (on glass) averaged from the 20 single nanocrystals for each nanocrystal size. For a nanocrystal with  $D=5.2$  nm,  $I_{\text{gold}}/I_{\text{glass}}$  reaches about 5 at around 500 nm, which means that the PL intensity on a rough Au surface is enhanced about five times more than that on glass. Note that  $I_{\text{gold}}/I_{\text{glass}}$  decreases with a decrease of the nanocrystal and  $I_{\text{gold}}/I_{\text{glass}}$  for a nanocrystal of  $D=4.0$  and  $2.4$  nm is less than unity at all excitation wavelengths; that is, PL quenching occurs. This indicates that the PL enhancement is sensitive to the nanocrystal size.

Three-dimensional (3D) finite-difference time domain (FDTD) method simulations were used to reveal the mechanism of PL enhancement.<sup>14</sup> Atomic force microscopy images show that rough Au surfaces are composed of an assembly of hemispherical particles with lateral sizes of 20–50 nm and peaks and valleys of roughly 15 nm.<sup>12</sup> The inset of Fig. 2(a) shows a 3D model of rough Au surface for the FDTD simulations. The complex dielectric constants of Au are approximated using the Drude model, and  $x$ -polarized plane-wave illumination ( $\lambda=532$  nm) is applied in this simulation. Figure 2(a) shows plan view of the simulated electric field intensity distributions at  $z=5$  nm plane. The electric field strength is concentrated and enhanced at the edges of the metal hemispheres in parallel with the polarization direction. From this result, the maximum field intensity reached is 25 times that in air.

Figure 2(b) shows dependence of the electric field intensity on the incident polarization angle at the position indicated in Fig. 2(a). The electric field intensity depends strongly on the polarization angle and shows clear oscillation behavior with a period of  $180^\circ$ , which is similar to the experimental result [see Fig. 1(c)]. Furthermore, the simulated field intensity is plotted as a function of the illumination wavelength in Fig. 2(c). The significant resonance of the

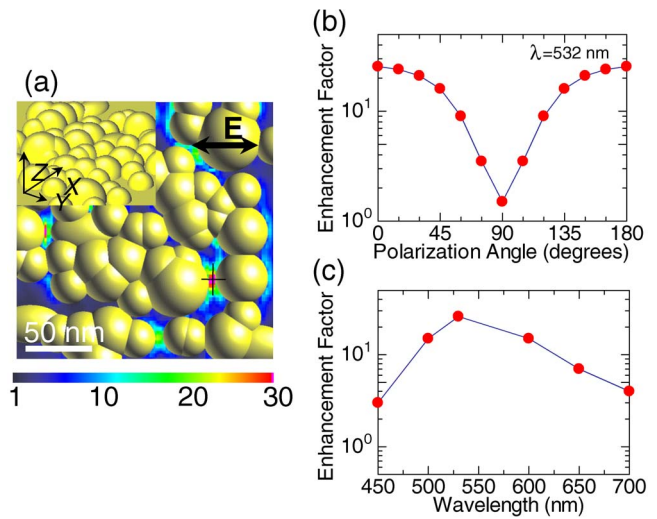


FIG. 2. (Color online) (a) Numerical simulation of the local electric field on a rough Au surface. Inset shows FDTD model of rough Au surface. The incident electric field ( $\lambda=533$  nm) is  $x$  polarized with a value of unity in air. (b) Polarization dependence of the simulated local electric field around the Au hemispheres. (c) Local electric-field intensity as a function of the incident wavelength.

electric field enhancement near 530 nm is consistent with the PL enhancement in Fig. 1(d). The wavelength of the field enhancement maximum roughly corresponds to the absorption peak of the Au-plasmon resonance.<sup>15</sup> The resonance behavior and polarization dependence of the PL intensities provide direct evidence that the PL enhancement arises from the local electric field enhancement by the surface plasmon excitation.

The PL intensity on the Au surface is determined mainly by two processes: quenching of the excited state caused by the energy transfer to the metal surface and enhancement of the absorption and radiative emission rate due to the surface plasmon-induced electric field. In this case, the PL enhancement factor ( $I_{\text{gold}}/I_{\text{glass}}$ ) in Fig. 1(d) is given by<sup>16</sup>

$$I_{\text{gold}}/I_{\text{glass}} \approx \frac{P(\omega_{\text{emis}})P(\omega_{\text{laser}})\gamma_{\text{rad}}}{\gamma_{\text{metal}}}, \quad (1)$$

where  $P(\omega_{\text{laser}})$  and  $P(\omega_{\text{emis}})$  are the electromagnetic enhancement factors for absorption and radiative emission on the metal surface, respectively, and  $\gamma_{\text{rad}}$  and  $\gamma_{\text{metal}}$  are the radiative recombination rate and nonradiative energy transfer rate from the nanocrystals to the metal surface, respectively.

The inset of Fig. 3 shows the PL decay curves of nanocrystals ( $D=5.2$  nm) on glass and Au surfaces. The fast-decay lifetimes of nanocrystals on a Au surface ( $\tau_{\text{PL,metal}} \sim 200$  ps) are much shorter than those on glass ( $\tau_{\text{PL}} \sim 1/\gamma_{\text{rad}} \sim 11$  ns). The PL lifetimes on a Au surface are determined by the energy transfer rate from the nanocrystals to the metal surface  $\gamma_{\text{metal}}$  because  $\gamma_{\text{metal}}$  is much larger than  $\gamma_{\text{rad}}$  in  $1/\tau_{\text{PL,metal}} = \gamma_{\text{rad}} + \gamma_{\text{metal}}$ . Since the ratio of the decay rates  $\gamma_{\text{rad}}/\gamma_{\text{metal}}$  is about  $1/50$  ( $=200$  ps/ $11$  ns) for the largest nanocrystals ( $D=5.2$  nm), drastic quenching of the PL intensity is thought to occur on the Au surface. However, fivefold PL enhancement is observed at around 500 nm experimentally [see Fig. 1(d)]. Therefore, the PL enhancement factor of  $P(\omega_{\text{emis}})P(\omega_{\text{laser}})$  is evaluated to be about 250 times that on the glass surface using Eq. (1). Since the parameters in Eq. (1) other than  $P(\omega_{\text{laser}})$  do not depend on the excitation con-

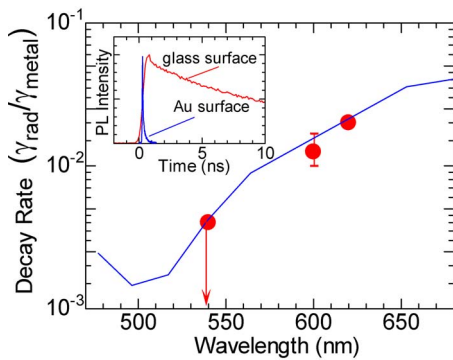


FIG. 3. (Color online) Nanocrystal size dependent decay rates. Inset shows PL decay curves of nanocrystals on rough Au surface and on glass in macroscopic ensemble-averaged experiments. Measured (closed circles) and calculated decay rates (solid curve) as a function of the emission wavelength.

ditions, the enhancement parameter  $P(\omega_{\text{laser}})$  can be obtained experimentally from the difference in the maximum and minimum values of  $I_{\text{gold}}/I_{\text{glass}}$ . Based on the polarization-dependence experiments in Fig. 1(c), the value of  $P(\omega_{\text{laser}})$  is about 20. This value is consistent with the result of the FDTD simulation ( $\sim 25$ ), as shown in Fig. 2(b).

The PL enhancement or quenching is determined by the balance between the decay rate  $\gamma_{\text{rad}}/\gamma_{\text{metal}}$  and the electromagnetic enhancement factor. Figure 3 shows the decay rate  $\gamma_{\text{rad}}/\gamma_{\text{metal}}$  as a function of the emission wavelength. The decay times were derived from the convoluted curve fitting analysis that considered the instrument response. The results give the upper limit of the decay time for nanocrystals ( $D=2.4$  nm) on Au because of the finite temporal resolution. The decay rates  $\gamma_{\text{rad}}/\gamma_{\text{metal}}$  of nanocrystals with  $D=4.0$  and  $2.4$  nm are about  $1/80$  ( $=90$  ps/ $7.5$  ns) and  $<1/250$  ( $\leq 20$  ps/ $4.6$  ns), respectively. The emission wavelength changes from  $620$  to  $540$  nm as the nanocrystal size decreases from  $5.2$  to  $2.4$  nm. The decay rate decreases drastically with the smaller nanocrystal whose emission wavelength approaches to the plasmon resonance ( $\sim 530$  nm). The experimental result shows that the decay rate is mainly determined by the energy transfer process from the nanocrystal to the Au surface.

Within the framework of the dipole approximation, the nonradiative energy transfer rate  $\gamma_{\text{metal}}$  is determined mainly by two factors: the distance  $d$  from a nanocrystal to the Au hemisphere and the emission energy of the nanocrystal relative to the surface plasmon resonance.  $\gamma_{\text{metal}}$  is proportional to  $1/d^6$  at large distances, whereas it becomes close to the surface-transfer law  $\gamma_{\text{metal}} \propto 1/\Delta^4$  when a gap  $\Delta$  between the surfaces of the CdSe core and Au hemisphere becomes small and Au hemisphere is much larger than the nanocrystal.<sup>16,17</sup> In this case, the decay rate is given by

$$\gamma_{\text{rad}}/\gamma_{\text{metal}} \propto \omega_{\text{emis}}^3 \Delta^4 \text{Im} \left[ \frac{\epsilon_{\text{Au}}(\omega_{\text{emis}}) + 2\epsilon_0}{\epsilon_{\text{Au}}(\omega_{\text{emis}}) - \epsilon_0} \right], \quad (2)$$

where  $\Delta$  is a constant gap consisting of the ZnS barrier and TOPO ( trioctylphosphine oxide) surfactant independent of

the nanocrystal core size,  $\epsilon_{\text{Au}}(\omega_{\text{emis}})$  is the dielectric constant of Au from empirical tables,<sup>18</sup> and  $\epsilon_0$  is the background dielectric constant. Figure 3 shows the calculated decay rate as a function of the emission wavelength (solid line) and its tendency is consistent with the experimental result. Consequently, the nonradiative rate increases due to the resonant energy transfer from the excited state of a nanocrystal to the localized plasmon. Therefore, the experimentally observed change from PL enhancement to quenching depending on size can be explained by an increase in the rates of plasmon induced resonant energy transfer in the smaller nanocrystals.

In summary, we showed the PL enhancement of single CdSe/ZnS nanocrystals on rough metal surfaces depending on the excitation wavelength and polarization angle and it arises from local field enhancement induced by surface plasmons. A single nanocrystal spectroscopy and time-resolved spectroscopy reveal the roles of excitation process and energy transfer process in the PL enhancement and quenching. Excitation polarization-dependent PL enhancement and quenching were observed, and they were controlled by the balance between the resonant energy transfer rate from a nanocrystal to the Au surfaces and the electric field enhancement.

The authors thank Mr. T. Yasui and Professor T. Saiki for supporting the FDTD simulation. This work was supported by JSPS (No. 18340089).

- <sup>1</sup>V. L. Colvin, M. C. Schlamp, and A. P. Alivisatos, *Nature (London)* **370**, 354 (1994).
- <sup>2</sup>V. I. Klimov, A. A. Mikhailovsky, Su Xu, A. Malko, J. A. Hollingsworth, C. A. Leatherdale, H.-J. Eisler, and M. G. Bawendi, *Science* **290**, 314 (2002).
- <sup>3</sup>A. J. Nozik, *Physica E (Amsterdam)* **14**, 115 (2002).
- <sup>4</sup>K. T. Shimizu, W. K. Woo, B. R. Fisher, H. J. Eisler, and M. G. Bawendi, *Phys. Rev. Lett.* **89**, 117401 (2002).
- <sup>5</sup>O. Kulakovich, N. Strekal, A. Yaroshevich, S. Maskevich, S. Gaponenko, I. Nabiev, U. Woggon, and M. Artemyev, *Nano Lett.* **2**, 1449 (2002).
- <sup>6</sup>B. Nikoobakht, C. Burda, M. Braun, M. Hun, and M. A. El-Sayed, *Photochem. Photobiol.* **75**, 591 (2002).
- <sup>7</sup>J.-H. Song, T. Atay, S. Shi, H. Urabe, and A. V. Nurmikko, *Nano Lett.* **5**, 1557 (2005).
- <sup>8</sup>J. S. Biteen, D. Pacifici, N. S. Lewis, and H. A. Atwater, *Nano Lett.* **5**, 1768 (2005).
- <sup>9</sup>J. Zhang, Y.-H. Ye, X. Wang, P. Rochon, and M. Xiao, *Phys. Rev. B* **72**, 201306(R) (2005).
- <sup>10</sup>V. K. Komarala, Y. P. Rakovich, A. L. Bradley, S. J. Byrne, Y. K. Gun'ko, N. Gaponik, and A. Eychmüller, *Appl. Phys. Lett.* **89**, 253118 (2006).
- <sup>11</sup>K. Okamoto, S. Vyawahare, and A. Scherer, *J. Opt. Soc. Am. B* **23**, 1674 (2006).
- <sup>12</sup>Y. Ito, K. Matsuda, and Y. Kanemitsu, *Phys. Rev. B* **75**, 033309 (2007).
- <sup>13</sup>P. Anger, P. Bharadwaj, and L. Novotny, *Phys. Rev. Lett.* **96**, 113002 (2006).
- <sup>14</sup>S. A. Maier, P. G. Kik, and H. A. Atwater, *Appl. Phys. Lett.* **81**, 1714 (2002).
- <sup>15</sup>F. Hache, D. Richard, and C. Flytzanis, *J. Opt. Soc. Am. B* **3**, 1647 (1986).
- <sup>16</sup>A. O. Govorov, G. W. Bryant, W. Zhang, T. Skeini, J. Lee, N. Kotov, J. M. Slocik, and R. R. Naik, *Nano Lett.* **6**, 984 (2006).
- <sup>17</sup>B. N. J. Persson and N. D. Lang, *Phys. Rev. B* **26**, 5409 (1982).
- <sup>18</sup>E. D. Palik, *Handbook of Optical Constants of Solids* (Academic, New York, 1985).